Correlation energy of the paramagnetic electron gas at the thermodynamic limit

Sam Azadi,[1,*] N. D. Drummond,[2] and Sam M. Vinko[1,3]

[1] *Department of Physics, Clarendon Laboratory, University of Oxford, Parks Road, Oxford OX1 3PU, United Kingdom*

[2] *Department of Physics, Lancaster University, Lancaster LA1 4YB, United Kingdom*

[3] *Central Laser Facility, STFC Rutherford Appleton Laboratory, Didcot OX11 0QX, United Kingdom*

(Dated: March 15, 2023)

The variational and diffusion quantum Monte Carlo methods are used to calculate the correlation energy of the paramagnetic three-dimensional homogeneous electron gas at intermediate to high density. Ground state energies in finite cells are determined using Slater-Jastrow-backflow trial wave functions, and finite-size errors are removed using twist-averaged boundary conditions and extrapolation of the energy per particle to the thermodynamic limit of infinite system size. Our correlation energies in the thermodynamic limit are more accurate than previous results. The present diffusion quantum Monte Carlo energies, together with our recently reported [Phys. Rev. B **105**, 245135 (2022)] results at low density, are used to parameterize the correlation energy of the electron gas using a functional form that satisfies the exact asymptotic behavior at high density.

Introduction. The pairwise Coulomb repulsion between electrons results in many-body correlations in electronic systems such as the homogeneous electron gas (HEG) [1, 2]. The so-called correlation energy is a negative correction to the mean-field Hartree-Fock energy. Although the correlation energy is usually only a small percentage of the total energy of an electronic system, it is crucial for an accurate description of chemical and electronic properties [3–5]. Unfortunately, it is also the most complicated part of the energy to calculate accurately.

The three-dimensional (3D) HEG plays a crucial role in our understanding of the nature of electronic correlation in real materials [6–8]. Moreover, the HEG is one of the most important models for our understanding of bulk systems under extreme conditions, such as warm dense matter, which is an exotic, highly compressed state of matter that exists between solid and plasma phases at high temperatures [9–11]. The correlation energy of the 3D HEG as a function of density [12–14] is a fundamental element in the description of the electronic properties of real systems by density functional theory (DFT) [15, 16]. However, calculating the correlation energy accurately requires many-body wave function-based methods [17] such as quantum Monte Carlo (QMC) techniques [18–25]. The variational (VMC) and diffusion quantum Monte Carlo (DMC) methods [18, 26] are stochastic approaches for obtaining expectation values of quantum operators. These techniques are especially efficient for calculating the ground state energies of interacting fermions. The main object is an approximate trial wave function, whose accuracy governs the final energy and intrinsic statistical fluctuations in the simulations.

The DMC simulations of Ceperley and Alder [18] presented important data connecting the high- and low-density regimes of the correlation energy of the 3D HEG. Their data have been used in parameterizations of the correlation energy over a wide density range and are frequently used in DFT calculations. Well-known parameterizations that make use of Ceperley and Alder's results were provided by Perdew and Zunger (PZ81) [27], Vosko, Wilk, and Nusair (VWN80) [28], and Perdew and Wang (PW92) [29], among others. The PW92 functional includes five parameters, two determined from analytic high-density constraints and three by fitting to the QMC data. A density parameter interpolation (DPI) [12], which was constructed by imposing four high-density and three low-density constraints on a seven-parameter functional form, provided a check based purely on the satisfaction of the exact constraints. Spink *et al.* [23] performed QMC calculations for spin-unpolarized and spin-polarized 3D HEGs over the high- and intermediate-density ranges, which can be regarded as the most accurate QMC data reported so far. In the present work, we provide new QMC data for the correlation energy of the paramagnetic (i.e., spin unpolarized) 3D HEG, which are lower than previously reported results. We use long-range backflow correlations to make fixed-node errors more consistent between different cell sizes. Instead of using the analytic finite-size corrections, we extrapolate our results to infinite system size which provides more accurate results at the thermodynamic limit [1]. QMC energies in finite simulation cells obey the variational principle and it is reasonable to assume that the QMC energy per particle extrapolated to infinite system size is also an upper bound on the true energy per particle. Hence the fact that our energies are lower than previous works strongly suggests that our results are more accurate.

We have used the VMC and DMC methods to obtain 3D HEG correlation energies at different densities. In the VMC method, parameters in a trial wave function are optimized according to the variational principle, with energy expectation values calculated by Monte Carlo in-

* sam.azadi@physics.ox.ac.uk

tegration in the $3N$-dimensional space of electron position vectors. In the DMC method, the imaginary-time Schrödinger equation is used to evolve a statistical ensemble of electronic configurations towards the ground state. Fermionic antisymmetry is maintained by the fixed-phase approximation, in which the complex phase of the wave function is constrained to equal that of an approximate trial wave function optimized within VMC.

The simplest fermionic wave function is a Slater determinant, which describes exchange effects but not correlation. Multideterminant wave functions and pairing (geminal) wave functions [30] can also be used. The most efficient method of going beyond the Slater wave function is to multiply it by a Jastrow factor $\exp(J)$, resulting in a Slater-Jastrow wave function [20, 21]. The Jastrow factor usually depends explicitly on the distances between particles, introducing correlation into the wave function. The Jastrow factor is positive everywhere and symmetric with respect to the exchange of indistinguishable particles, so it does not change the nodal surface defined by the rest of the wave function. By evaluating the orbitals in the Slater determinant at quasiparticle coordinates $\mathbf{X}$, which are functions of all the electron positions, we introduce a backflow transformation [31, 32], and the resulting wave function is referred to as a Slater-Jastrow-backflow (SJB) wave function.

Trial wave function. We used a SJB trial spatial wave function $\Psi(\mathbf{R}) = e^{J(\mathbf{R})}S(\mathbf{X}(\mathbf{R}))$ for all the systems we have studied, where $\mathbf{R} = (\mathbf{r}_1, \ldots, \mathbf{r}_N)$ is the $3N$-dimensional vector of electron coordinates. The antisymmetric Slater part S is a product of determinants of single-particle orbitals for spin-up and spin-down electrons. The single-particle orbitals in S are of the free-electron form $\psi_{\mathbf{k}}(\mathbf{r}) = \exp(i\mathbf{k}\cdot\mathbf{r})$, where wavevector $\mathbf{k}$ is a reciprocal lattice vector of the simulation cell offset by twist vector $\mathbf{k}_\mathrm{s}$, where $\mathbf{k}_\mathrm{s}$ lies in the supercell Brillouin zone. The Jastrow exponent, which is symmetric under electron exchange, takes the form

$$\begin{aligned} J &= U + P + H \\ &= \sum_{i<j} u(r_{ij}) + \sum_{i<j} p(\mathbf{r}_{ij}) + \sum_{i<j<k} h(r_{jk}, r_{ik}, r_{ij}), \end{aligned} \tag{1}$$

where

$$u(r) = \sum_{l=0}^{N_u} \alpha_l r^l (r - L_u)^C \Theta(L_u - r), \tag{2}$$

where r is the minimum-image distance between two electrons, the cutoff length L_u is less than or equal to the radius of the largest sphere that can be inscribed in the Wigner-Seitz cell of the simulation cell, $C = 3$ specifies how smooth the function is at the cutoff length, Θ is the Heaviside step function, and $\{\alpha_l\}$ are optimizable parameters, which differ for parallel- and antiparallel-spin electrons. To satisfy the Kato cusp conditions [33, 34], we fix $\alpha_1 = \Gamma/(-L_u)^C + \alpha_0 C/L_u$, where $\Gamma = 1/2$ for opposite-spin electrons and $\Gamma = 1/4$ for same-spin electrons. We chose $N_u = 8$. The p term has the symmetry of the simulation-cell Bravais lattice and allows a description of correlation in the "corners" of the simulation cell. Its form is

$$p(\mathbf{r}) = \sum_A a_A \sum_{\mathbf{G}\in A^+} \cos(\mathbf{G}\cdot\mathbf{r}), \tag{3}$$

where A represents a star of symmetry-equivalent, nonzero, simulation-cell reciprocal-lattice vectors $\mathbf{G}$, and A^+ is a subset of A that consists of one out of each $\pm\mathbf{G}$ pair. The $\{a_A\}$ are optimizable parameters. We used 46 stars of $\mathbf{G}$ vectors in p. The Jastrow also includes symmetric three-electron terms [35, 36]

$$\begin{aligned} h(r, r', r'') &= \sum_{l=0}^{N_h}\sum_{m=0}^{N_h}\sum_{n=0}^{N_h} c_{lmn} r^l (r')^m (r'')^n \\ &\quad \times (r - L_h)^C (r' - L_h)^C (r'' - L_h)^C \\ &\quad \times \Theta(L_h - r)\Theta(L_h - r')\Theta(L_h - r'') \end{aligned} \tag{4}$$

where L_h is a cutoff length and c_{lmn} are linear parameters. Constraints were placed on the linear parameters to ensure that h is cuspless. We chose $N_h = 4$. Different h terms, meaning different $\{c_{lmn}\}$, may be used for electron triplets involving different combinations of spins. However, in this work, the parameters in the three-electron Jastrow factors were constrained to be independent of spin.

Including a backflow transformation in the trial wave function, the Slater part of the wave function S is evaluated at transformed "quasiparticle" coordinates $\mathbf{X}(\mathbf{R}) = \mathbf{R} + \boldsymbol{\xi}(\mathbf{R})$, where

$$\boldsymbol{\xi}_i(\mathbf{R}) = \sum_{j\neq i} \eta(r_{ij})\mathbf{r}_{ij} + \sum_{j\neq i} \boldsymbol{\pi}(\mathbf{r}_{ij}) \tag{5}$$

is the backflow displacement of electron i. η is a cuspless, smoothly truncated, isotropic polynomial function of minimum-image electron-electron distance r_{ij}. The polynomial coefficients are optimizable parameters, and are different for parallel- and antiparallel-spin electrons [32]. The form of $\eta(r)$ is mathematically equivalent to that of the Jastrow $u(r)$ term [Eq. (2), with $\Gamma = 0$ for same-spin electrons and optimizable for opposite-spin electrons]. Typically we used $N_\eta = 8$ in the polynomial expansions. The $\boldsymbol{\pi}$ term has the form of the gradient of a Jastrow p term [Eq. (3)]:

$$\boldsymbol{\pi}(\mathbf{r}) = -\sum_A c_A \sum_{\mathbf{G}\in A^+} \sin(\mathbf{G}\cdot\mathbf{r})\,\mathbf{G}, \tag{6}$$

where the c_A are optimizable parameters. As the gradient of a scalar field, the $\boldsymbol{\pi}$ term is irrotational. We used 44 stars of $\mathbf{G}$ vectors in $\boldsymbol{\pi}$. The backflow parameters were allowed to depend on the spins of the electron pairs.

The wave functions were optimized by variance minimization [37, 38] followed by energy minimization [39].

The CASINO package was used for all our QMC calculations [40].

Finite-size effects. Monte Carlo-sampled canonical ensemble twist-averaged (TA) boundary conditions were used to reduce quasirandom single-particle finite-size errors in total energies due to momentum quantization effects [41–45]. The Hartree-Fock kinetic and exchange energies were used as control variates to improve the precision of the twist-averaged energy. Systematic finite-size errors due to the use of the Ewald interaction rather than $1/r$ to evaluate the interaction between each electron and its exchange-correlation hole and the incomplete description of long-range two-body correlations were removed by fitting $E(N) = E(\infty) + b/N$ to the TA DMC energy per particle at different system sizes [46]. Unlike the previous work of Spink *et al.* [23], we do not rely on analytic finite-size correction formulas [43, 46], but instead use the analytic results to provide the exponents used in finite-size extrapolation formulas. All our calculations were performed using face-centered cubic simulation cells, maximizing the distance between each particle and its closest periodic image.

At very high density $r_s \ll 1$, systematic finite-size effects are more challenging. In this regime, the QMC energy is close to the Hartree-Fock energy, and hence the QMC energy per particle initially shows the Hartree-Fock $O(N^{-2/3})$ scaling with system size [43], before eventually crossing over to the asymptotic $O(N^{-1})$ scaling when the finite-size error becomes small compared with the correlation energy.

Correlation energies. We studied the paramagnetic 3D HEG at density parameters $r_s = 0.5$, 0.75, 1, 2, 3, 4, 5, 7, 10, and 20. For each density, QMC calculations were performed for simulation cells with $N = 130$, 226, and 338 electrons. Our DMC energies were extrapolated linearly to zero time step τ, with the target walker population being varied in inverse proportion to the time step [47]. The difference between the twist-averaged DMC energy at small r_s (i.e., $r_s \leq 1.0$) obtained with a time step $\tau = 0.02 r_s^2$ and the energy at zero time step is not statistically significant. The same behavior was observed at large r_s with $\tau = 0.01 r_s^2$. The energies and variances calculated using SJB wave functions for different system sizes are reported in the Supplemental Material [47]. The correlation energy is defined as the difference between the Hartree-Fock energy per electron [which is $E_{\rm HF} = 3(9\pi/4)^{2/3}/(10r_s^2) - 3(9\pi/4)^{1/3}/(4\pi r_s)$ for the paramagnetic HEG] and the exact ground-state energy per electron, where the latter is approximated by our SJB-DMC results extrapolated to the limit of infinite system size.

Table I summarizes the contribution of each term of the trial wave function to the correlation energy per particle in a simulation cell containing $N = 54$ electrons. We considered two systems with $r_s = 0.5$ and $r_s = 20$. Figure 1 shows the improvements in the VMC and DMC correlation energies resulting from the inclusion of different terms in the Jastrow and backflow functions.

Full configuration interaction quantum Monte Carlo (FCIQMC) calculations for $N = 54$ electrons in simple cubic cells subject to periodic boundary conditions (PBC) find the ground state energies of the 3D HEG at density parameters $r_s = 0.5$ and 1 to be 3.2202(2) and 0.5300(3) Ha/elec., respectively [24]. Using the same simple cubic cell with the same system size ($N = 54$) and PBC, our SJB-DMC total energies for $r_s = 0.5$ and 1 are 3.220897(3) and 0.529791(2) Ha/elec., respectively. These DMC energies were obtained using time steps of 0.005 and 0.01 a.u, respectively. Our results indicate that the SJB-DMC and FCIQMC energies are within errors of each other. Our Jastrow-Backflow functions are available to be downloaded from Ref. [47]. According to Spink *et al.* [23], the TA VMC energy of the spin-unpolarized 3D HEG at $r_s = 0.5$ at a system size of $N = 118$ is 3.41378(2) Ha/elec. Our TA VMC simulation for the same system size yields the energy as 3.412460(4) Ha/elec., which is ~ 36 meV/elec. lower, because of the inclusion of the $\boldsymbol{\pi}$ term in our work.

TABLE I. TA VMC and DMC correlation energies for $N = 54$ system size obtained using different terms in the Jastrow exponent and using both SJB and SJ wave functions. Where Jastrow terms are not specified, U, P, and H terms were used; where the backflow terms are not specified, η and $\boldsymbol{\pi}$ terms were used.

Wave fn	Correlation energy (eV/elec.)			
	$r_s = 0.5$		$r_s = 20$	
	VMC	DMC	VMC	DMC
SJ(U)	−2.5112(3)	−2.5684(4)	−0.311717(2)	−0.317465(4)
SJ($U + H$)	−2.5161(3)	−2.5680(5)	−0.313798(3)	−0.317469(5)
SJ	−2.5381(3)	−2.5685(4)	−0.314464(3)	−0.317492(5)
SJB(η)	−2.6056(5)	−2.6166(5)	−0.319082(3)	−0.320579(5)
SJB	−2.6331(3)	−2.6366(4)	−0.319346(2)	−0.320756(4)

Our VMC and DMC energies extrapolated to the limit of infinite system size are listed in Table II. To obtain the best linear fit and reduce the noise in the energies as a function of the number of particles N, a larger number of twists was used for higher densities and smaller system sizes. The smallest and largest number of twists were 120 and 10^4, respectively. Our results show an unexpected trend of decreasing VMC-DMC difference with increasing system size. This trend can be made plausible by an extreme example. If an uncorrelated Slater determinant trial wave function were used then VMC would reduce to Hartree-Fock theory with an $O(N^{-2/3})$ finite-size error in the energy per particle (see Table I of the Supplemental Material [47]), whereas the fixed-node DMC energy would include long-range two-body correlations and the finite-size error would go as $O(N^{-1})$. Hence VMC and DMC energies may behave very differently as functions of system size. Comparing our infinite-system VMC and DMC results with the DMC energies of Spink *et al.* [23] demonstrates not only the improvement of the trial wave function due to the inclusion of long-range $\boldsymbol{\pi}$ backflow terms, but also the importance of removing finite-size

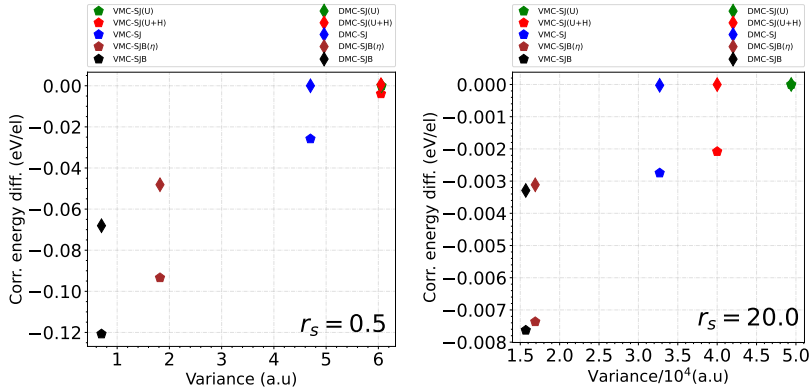

FIG. 1. Twist averaged VMC and DMC correlation energies at system size $N = 54$ as a function of variance, relative to the correlation energy with a Slater-Jastrow (SJ) wave function in which the Jastrow factor only contains the isotropic two-body term U. Results are shown at density parameters $r_s = 0.5$ (left panel) and 20 (right panel).

effects by extrapolation rather than relying on analytic correction formulas.

TABLE II. TA VMC and DMC energies of the 3D HEG extrapolated to the thermodynamic limit from different system sizes (N = 130, 226, and 338), compared with the DMC results of Spink *et al.* [23], and Ceperley and Alder [18]. Our DMC energies have been extrapolated to zero time step.

	Total energy (Ha/elec.)			
r_s	VMC	DMC		
	Pres. wk.	Pres. wk.	Spink *et al.*	Ceperley & Alder
0.5	3.4255(1)	3.42541(8)	3.43011(4)	...
0.75	1.28625(5)	1.28620(5)	...	...
1.0	0.58643(4)	0.58640(2)	0.58780(1)	0.5870(5)
2.0	0.00195(2)	0.001917(9)	0.002380(5)	0.002050(2)
3.0	−0.06728(1)	−0.067309(9)	−0.067075(4)	...
4.0	−0.07767(1)	−0.07771(1)	...	...
5.0	−0.07594(1)	−0.07597(1)	−0.075881(1)	−0.07560(5)
7.0	−0.066304(5)	−0.066348(2)	...	...
10.0	−0.053503(2)	−0.053527(5)	−0.0535116(5)	−0.0533750(2)
20.0	−0.031720(6)	−0.031755(3)	−0.0317686(5)	−0.0316450(1)

Table III compares our VMC and DMC results for the correlation energy with the PZ81 [27], VWN80 [28], PW92 [29], and DPI [12] parameterizations, as well as the DMC data of Spink *et al.* [23]. Our correlation energies are the lowest. Even at the high density $r_s = 0.5$ our DMC correlation energy is lower than the DPI parameterization by −16 meV/elec.

Following Ceperley [21], we fit

$$E_c(r_s) = \frac{\gamma}{1 + \beta_1\sqrt{r_s} + \beta_2 r_s} \qquad (7)$$

to our SJB-DMC correlation energies (Fig. 2). The fitting parameters γ, β_1, and β_2 are −0.151(5) Ha 1.18(7), and 0.338(5), respectively. The χ^2 value of the fit is 307.48 per degree of freedom. Equation (7) is accurate for large r_s, as we have shown in our recent work on the low-density phase diagram of the HEG, where our DMC correlation energies for $30 \le r_s \le 100$ were fitted to Eq. (7) giving a χ^2 per degree of freedom of 0.521 [1]. We found that the χ^2 per degree of freedom becomes 0.698 by fitting DMC correlation energies for $20 \le r_s \le 100$ to Eq. (7) and we found the fitting parameters γ, β_1, and β_2 to be −0.1278(55) Ha/elec., 0.897(53), and 0.299(12), respectively.

According to the all-orders perturbation theory of Gell-Mann and Brueckner [17] the correlation energy at high density is given by $E_c(r_s) = A\ln(r_s) + C + O(r_s\ln(r_s))$, where $A = \frac{1}{\pi^2}[1 - \ln(2)] \approx 0.0311$ Ha and $C \approx -0.0465$ Ha. The appearance of powers of $\ln(r_s)$ in this formula shows that the correlation energy is a nonanalytic function of r_s for $r_s \to 0$ and describes the failure of the naive perturbation approach. The constant term C is the sum of the second-order Onsager's exchange integral and a numerical constant caused by the sum over divergent contributions [48]. In practice, this asymptotic formula is accurate only for very small $r_s \ll 1$. We fitted our VMC and DMC correlation energies for $r_s = 0.5$, 0.75, and 1 to the Gell-Mann-Brueckner expression (Fig. 2). The fitting parameters are $A_{\rm VMC} = 0.0250(5)$ Ha, $C_{\rm VMC} = -0.06030(2)$ Ha, $A_{\rm DMC} = 0.0250(5)$ Ha, and $C_{\rm DMC} = -0.06040(1)$ Ha. The difference between the VMC and DMC fitting parameters is small because the random errors due to twist averaging at high density dominate. Figure 2 shows that at $r_s \le 0.1$ the correlation energy predicted by the Gell-Mann-Brueckner formula becomes smaller than VMC and DMC. One can include an additional term in the Gell-Mann-Brueckner expansion and write the high-density expansion of the correlation energy per electron as

$$E_c(r_s) = A\ln(r_s) + C + Br_s\ln(r_s) + O(r_s), \qquad (8)$$

where the exact value of the coefficient of $r_s\ln(r_s)$ is $B = 0.00922921$ [13]. We fitted our DMC correlation energies for $r_s = 0.5$, 0.75, 1.0, and 2.0 to the extended expansion, and we found that the fitting parameters A, C, and B are 0.0275(4), −0.06001(7), and −0.0031(2)

TABLE III. Correlation energies for the spin-unpolarized 3D HEG from the PZ81 [27], VWN80 [28], PW92 [29], and DPI [12] parameters, DMC (Spink *et al.* [23]), and this work (VMC and DMC).

r_s	Correlation energy (eV/elec.)						
	PZ81	VWN80	PW92	DPI	DMC (Spink *et al.*)	VMC	DMC
0.5	−2.069	−2.097	−2.085	−2.108	−1.996	−2.121(3)	−2.124(2)
0.75	...	...	...	...	...	−1.829(1)	−1.831(1)
1.0	−1.623	−1.633	−1.627	−1.637	−1.605	−1.642(1)	−1.6432(5)
2.0	−1.227	−1.219	−1.218	−1.215	−1.218	−1.2301(5)	−1.2310(2)
3.0	−1.013	−1.004	−1.005	−0.996	−1.010	−1.0159(3)	−1.0166(2)
4.0	...	...	...	...	...	−0.8758(3)	−0.8769(3)
5.0	−0.771	−0.766	−0.768	−0.755	−0.774	−0.7756(3)	−0.7764(3)
7.0	...	...	...	...	...	−0.6368(1)	−0.6380(1)
10.0	−0.505	−0.485	−0.505	−0.495	−0.510	−0.5098(1)	−0.5105(2)
20.0	−0.313	−0.302	−0.314	−0.308	−0.316	−0.3149(1)	−0.3159(1)

Ha/elec., respectively, with a χ^2 value of 3.52579.

TABLE IV. Fitting parameters of Eq. (9) in Hartree.

Fitting parameter	Value	Asymptotic std. err.
A (Ha/elec.)	0.000435098	0.0001665
C (Ha/elec.)	−0.00221852	0.0008169
B (Ha/elec.)	-3.02312×10^{-7}	1.493×10^{-7}
D (Ha/elec.)	−0.0134875	0.0006189
γ (Ha/elec.)	−0.077337	0.004517
β_1	0.470881	0.05071
β_2	0.262613	0.004956

We fitted all our DMC correlation energies for $0.5 \leq r_s \leq 100$, which are reported in this work and in our recently published paper [1], to Eq. (7) plus Eq. (8) and we found the χ^2 per degree of freedom to be 54.3. We searched for the best fit with the smallest χ^2 value and discovered that by adding a $r_s^{-3/4}$ term to the sum of Eqs. (7) and (8) the χ^2 value is reduced to 1.26. Hence, the DMC results indicate that the correlation energy

$$E_c(r_s) = A\ln(r_s) + C + Br_s\ln(r_s) + \frac{D}{r_s^{3/4}} + \frac{\gamma}{1+\beta_1\sqrt{r_s}+\beta_2 r_s}, \quad (9)$$

can describe the correlation energy of the 3D paramagnetic HEG within the density range $0.5 \leq r_s \leq 100$, which covers the high-, middle-, and low-density regimes. The fitting parameters are listed in Table IV.

In conclusion, we have performed VMC and DMC simulations using SJB trial wave functions to calculate the correlation energy of the paramagnetic 3D HEG at high and intermediate densities. We corrected finite-size errors by twist averaging and extrapolation to the thermodynamic limit. Our DMC energies obtained in this work, together with our previous low-density results reported in Ref. [1], have been used to parameterize the correlation energy of the spin unpolarized 3D HEG at high, intermediate, and low densities.

S.A. and S.M.V. acknowledge support from the UK EPSRC grants EP/P015794/1 and EP/W010097/1, the Royal Society, and PRACE (Partnership for Advanced Computing in Europe) for awarding us access to the High-Performance Computing Center Stuttgart, Germany, through the Project No. 2020235573.

[1] S. Azadi and N. D. Drummond, Phys. Rev. B **105**, 245135 (2022).
[2] G. Cassella, H. Sutterud, S. Azadi, N. D. Drummond, D. Pfau, J. S. Spencer, and W. M. C. Foulkes, Phys. Rev. Lett. **130**, 036401 (2023).
[3] P.-O. Löwdin, Phys. Rev. **97**, 1509 (1955).
[4] R. O. Jones, Rev. Mod. Phys. **87**, 897 (2015).
[5] R. M. Dreizler and E. K. U. Gross, *Density Functional Theory* (Springer-Verlag: Berlin, 1990).
[6] D. Pines and P. Noziéres, *The Theory of Quantum Liquids* (W.A. Benjamin, Inc., New York, 1966).
[7] G. Giuliani and G. Vignale, *Quantum Theory of the Electron Liquid* (Cambridge University Press, Cambridge, UK, 2005).
[8] P.-F. Loos and P. M. W. Gill, Wiley Interdiscip. Rev.: Comput. Mol. Sci. **6**, 410 (2016).
[9] T. Dornheim, S. Groth, T. Sjostrom, F. D. Malone, W. M. C. Foulkes, and M. Bonitz, Phys. Rev. Lett. **117**, 156403 (2016).
[10] S. Groth, T. Dornheim, T. Sjostrom, F. D. Malone,

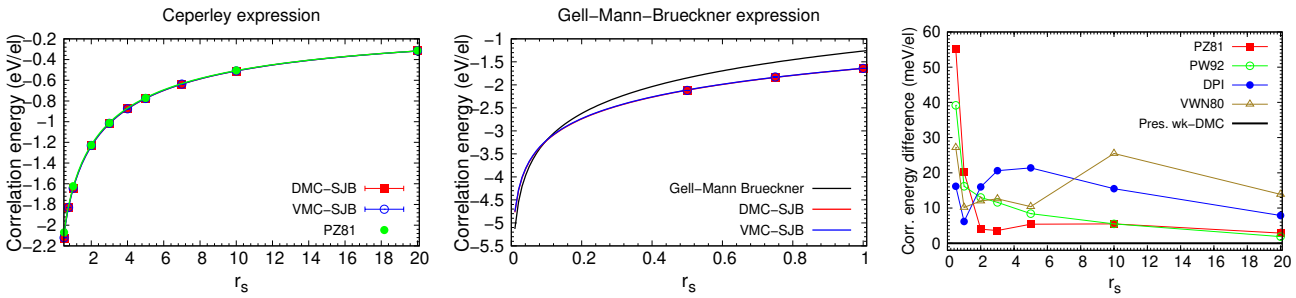

FIG. 2. Correlation energy of the spin-unpolarized 3D HEG as a function of r_s. (Left panel) The VMC and DMC correlation energies are fitted to Eq. (7) and are compared with the PZ81 [27] parameterization. (Middle panel) VMC and DMC correlation energies at high density (r_s = 0.5, 0.75, and 1) are fitted to Gell-Mann and Brueckner's asymptotic formula. The fitting parameters are presented in the main text. (Right panel) Difference between our DMC correlation energy (Pres. wk-DMC) and the PZ81 [27], VWN80 [28], PW92 [29], and DPI [12] DFT functionals.

W. M. C. Foulkes, and M. Bonitz, Phys. Rev. Lett. **119**, 135001 (2017).

[11] T. Dornheim, J. Vorberger, Z. A. Moldabekov, and P. Tolias, Phys. Rev. Res. **4**, 033018 (2022).

[12] J. Sun, J. P. Perdew, and M. Seidl, Phys. Rev. B **81**, 085123 (2010).

[13] P.-F. Loos and P. M. W. Gill, Phys. Rev. B **84**, 033103 (2011).

[14] P. Bhattarai, A. Patra, C. Shahi, and J. P. Perdew, Phys. Rev. B **97**, 195128 (2018).

[15] P. Hohenberg and W. Kohn, Phys. Rev. **136**, B864 (1964).

[16] W. Kohn and L. J. Sham, Phys. Rev. **140**, A1133 (1965).

[17] M. Gell-Mann and K. A. Brueckner, Phys. Rev. **106**, 364 (1957).

[18] D. M. Ceperley and B. J. Alder, Phys. Rev. Lett. **45**, 566 (1980).

[19] M. Holzmann and S. Moroni, Phys. Rev. Lett. **124**, 206404 (2020).

[20] D. M. Ceperley, G. V. Chester, and M. H. Kalos, Phys. Rev. B **16**, 3081 (1977).

[21] D. M. Ceperley, Phys. Rev. B **18**, 3126 (1978).

[22] S. Azadi, N. D. Drummond, and W. M. C. Foulkes, Phys. Rev. Lett. **127**, 086401 (2021).

[23] G. G. Spink, N. D. Drummond, and R. J. Needs, Phys. Rev. B **88**, 085121 (2013).

[24] J. J. Shepherd, G. H. Booth, A. Grüneis, , and A. Alavi, Phys. Rev. B **85**, 081103(R) (2012).

[25] M. Ruggeri, P. Ríos López, and A. Alavi, Phys. Rev. B **98**, 161105 (2018).

[26] W. M. C. Foulkes, L. Mitas, R. J. Needs, and G. Rajagopal, Rev. Mod. Phys. **73**, 33 (2001).

[27] J. P. Perdew and A. Zunger, Phys. Rev. B **23**, 5048 (1981).

[28] S. H. Vosko, L. Wilk, and M. Nusair, Can. J. Phys. **58**, 1200 (1980).

[29] J. P. Perdew and Y. Wang, Phys. Rev. B **45**, 13244 (1992).

[30] M. Marchi, S. Azadi, M. Casula, and S. Sorella, J. Chem. Phys. **131**, 154116 (2009).

[31] Y. Kwon, D. M. Ceperley, and R. M. Martin, Phys. Rev. B **58**, 6800 (1998).

[32] P. López Ríos, A. Ma, N. D. Drummond, M. D. Towler, and R. J. Needs, Phys. Rev. E **74**, 066701 (2006).

[33] T. Kato, Commun. Pure Appl. Math. **10**, 151 (1957).

[34] R. T. Pack and W. B. Brown, J. Chem. Phys. **45**, 556 (1966).

[35] Y. Kwon, D. M. Ceperley, and R. M. Martin, Phys. Rev. B **48**, 12037 (1993).

[36] P. López Ríos, P. Seth, N. D. Drummond, and R. J. Needs, Phys. Rev. E **86**, 036703 (2012).

[37] C. J. Umrigar, K. G. Wilson, and J. W. Wilkins, Phys. Rev. Lett. **60**, 1719 (1988).

[38] N. D. Drummond and R. J. Needs, Phys. Rev. B **72**, 085124 (2005).

[39] J. Toulouse and C. J. Umrigar, J. Chem. Phys. **126**, 084102 (2007).

[40] R. J. Needs, M. D. Towler, N. D. Drummond, P. López Ríos, and J. R. Trail, J. Chem. Phys. **152**, 154106 (2020).

[41] C. Lin, F. H. Zong, and D. M. Ceperley, Phys. Rev. E **64**, 016702 (2001).

[42] S. Azadi and W. M. C. Foulkes, J. Chem. Phys. **143**, 102807 (2015).

[43] N. D. Drummond, R. J. Needs, A. Sorouri, and W. M. C. Foulkes, Phys. Rev. B **78**, 125106 (2008).

[44] M. Holzmann, R. C. Clay, III, M. A. Morales, N. M. Tubman, D. M. Ceperley, and C. Pierleoni, Phys. Rev. B **94**, 035126 (2016).

[45] S. Azadi and W. M. C. Foulkes, Phys. Rev. B **100**, 245142 (2019).

[46] S. Chiesa, D. M. Ceperley, R. M. Martin, and M. Holzmann, Phys. Rev. Lett. **97**, 076404 (2006).

[47] Raw quantum Monte Carlo data for all the system sizes studied are presented in the supplemental material. the jastrow-backflow functions can be downloaded from github.com/arshamsam/HEG-Jastrow-Factors-.git.

[48] L. Onsager, L. Mittag, and M. J. Stephen, Ann. Phys. **473**, 71 (1966).